

Capturing the non-equilibrium state in light-matter-free-electron interactions through ultrafast transmission electron microscopy

Wentao Wang(汪文韬), Shuaishuai Sun(孙帅帅), Jun Li(李俊), Dingguo Zheng(郑丁国), Siyuan Huang(黄思远), Huanfang Tian(田焕芳), Huaixin Yang(杨槐馨), and Jianqi Li(李建奇)
Citation: Chin. Phys. B, 2024, 33 (**1**): 010701. DOI: 10.1088/1674-1056/ad0141
Journal homepage: http://cpb.iphy.ac.cn; http://iopscience.iop.org/cpb

What follows is a list of articles you may be interested in

Design of a novel correlative reflection electron microscope for *in-situ* real-time chemical analysis

Tian-Long Li(李天龙), Zheng Wei(魏征), and Wei-Shi Wan(万唯实)
Chin. Phys. B, 2021, 30 (**12**): 120702. DOI: 10.1088/1674-1056/ac0522

Design of an ultrafast electron diffractometer with multiple operation modes

Chun-Long Hu(胡春龙), Zhong Wang(王众), Yi-Jie Shi(石义杰), Chang Ye(叶昶), and Wen-Xi Liang(梁文锡)
Chin. Phys. B, 2021, 30 (**9**): 090701. DOI: 10.1088/1674-1056/ac11cd

Ultrafast structural dynamics using time-resolved x-ray diffraction driven by relativistic laser pulses

Chang-Qing Zhu(朱常青), Jun-Hao Tan(谭军豪), Yu-Hang He(何雨航), Jin-Guang Wang(王进光), Yi-Fei Li(李毅飞), Xin Lu(鲁欣), Ying-Jun Li(李英骏), Jie Chen(陈洁), Li-Ming Chen(陈黎明), and Jie Zhang(张杰)
Chin. Phys. B, 2021, 30 (**9**): 098701. DOI: 10.1088/1674-1056/ac0baf

Ultrafast electron microscopy in material science

Huaixin Yang(杨槐馨), Shuaishuai Sun(孙帅帅), Ming Zhang(张明), Zhongwen Li(李中文), Zian Li(李子安), Peng Xu(徐鹏), Huanfang Tian(田焕芳), Jianqi Li(李建奇)
Chin. Phys. B, 2018, 27 (**7**): 070703. DOI: 10.1088/1674-1056/27/7/070703

Ultrafast structural dynamics studied by kilohertz time-resolved x-ray diffraction

Guo Xin (郭鑫), Jiang Zhou-Ya (江舟亚), Chen Long (陈龙), Chen Li-Ming (陈黎明), Xin Jian-Guo (辛建国), Peter M. Rentzepis, Chen Jie (陈洁)
Chin. Phys. B, 2015, 24 (**10**): 108701. DOI: 10.1088/1674-1056/24/10/108701

TOPICAL REVIEW — States and new effects in nonequilibrium

Capturing the non-equilibrium state in light–matter–free-electron interactions through ultrafast transmission electron microscopy

Wentao Wang(汪文韬)[1,2,†], Shuaishuai Sun(孙帅帅)[1,†], Jun Li(李俊)[1], Dingguo Zheng(郑丁国)[1], Siyuan Huang(黄思远)[1,2], Huanfang Tian(田焕芳)[1], Huaixin Yang(杨槐馨)[1,2,4], and Jianqi Li(李建奇)[1,2,3,‡]

[1] *Beijing National Laboratory for Condensed Matter Physics, Institute of Physics, Chinese Academy of Sciences, Beijing* 100190, *China*
[2] *School of Physical Sciences, University of Chinese Academy of Sciences, Beijing* 100049, *China*
[3] *Songshan Lake Materials Laboratory, Dongguan* 523808, *China*
[4] *Yangtze River Delta Physics Research Center Co., Ltd., Liyang, Jiangsu* 213300, *China*

(Received 19 June 2023; revised manuscript received 28 September 2023; accepted manuscript online 9 October 2023)

Ultrafast transmission electron microscope (UTEM) with the multimodality of time-resolved diffraction, imaging, and spectroscopy provides a unique platform to reveal the fundamental features associated with the interaction between free electrons and matter. In this review, we summarize the principles, instrumentation, and recent developments of the UTEM and its applications in capturing dynamic processes and non-equilibrium transient states. The combination of the transmission electron microscope with a femtosecond laser via the pump–probe method guarantees the high spatiotemporal resolution, allowing the investigation of the transient process in real, reciprocal and energy spaces. Ultrafast structural dynamics can be studied by diffraction and imaging methods, revealing the coherent acoustic phonon generation and photo-induced phase transition process. In the energy dimension, time-resolved electron energy-loss spectroscopy enables the examination of the intrinsic electronic dynamics of materials, while the photon-induced near-field electron microscopy extends the application of the UTEM to the imaging of optical near fields with high real-space resolution. It is noted that light–free-electron interactions have the ability to shape electron wave packets in both longitudinal and transverse directions, showing the potential application in the generation of attosecond electron pulses and vortex electron beams.

Keywords: ultrafast transmission electron microscopy, non-equilibrium structural dynamics, photo-induced phase transition, free-electron–photon interactions

PACS: 07.78.+s, 87.15.ht, 42.50.Hz, 79.20.Uv **DOI:** 10.1088/1674-1056/ad0141

1. Introduction

The transmission electron microscope (TEM), capable of imaging atoms in solids with resolution as fine as 20 pm[1] and measuring spatial vibration energy with resolution as fine as 4.2 meV,[2] is an indispensable tool in modern scientific research. However, in the study of dynamical processes, the conventional TEM has time resolution only on the millisecond scale, which directly depends on the camera acquisition technique and is far from the scale required to observe many fundamental dynamical processes that occur on the scale of femtoseconds to picoseconds, such as the interplay between spin, charge, and phonons. A roundabout way to achieve better time resolution when using the TEM is to adopt the pump–probe method, which is expected to enable the observation of a number of important dynamic processes in advanced materials with high time resolution through control of the delay between the pump laser and pulsed electrons. Meanwhile, the advancement of laser technology allows the generation of laser pulses with a temporal width reaching a few attoseconds. Combining the TEM with a femtosecond laser via the pump–probe method provides a state-of-the-art setup referred to as the ultrafast transmission electron microscope (UTEM).[3–5]

As a versatile tool, the UTEM can operate in diffraction mode with a high transverse coherence length and in imaging mode with a high spatial resolution. Electron–phonon and phonon–phonon couplings in nanomaterials[6–8] and photo-induced phase transition[9] have been studied in real space and reciprocal space. The propagation of acoustic phonons in a film or nanowire will lead to morphological changes reflected in images.[10–12] Moreover, ultrafast dark-field imaging, which includes information in real and reciprocal spaces, directly reveals the structural phase transition in the nanometer domain and nanoscale sub-particle vibration.[13]

From the viewpoint of the energy dimension, the UTEM equipped with an electron energy-loss spectrometer can be used to reconstruct ultrafast electronic dynamics, such as the elemental charge transition in hematite,[14] the redshift of the plasmonic peak in carbon nanotubes[7] and boron nitride nanotubes,[8] with femtosecond temporal resolution. With meV energy resolution and a wide detection range from several to hundreds of electron volts, ultrafast electron energy-loss spectroscopy (EELS) has been applied in studies ranging from collective electron oscillation to nuclear electron dynam-

[†]These authors contributed equally.
[‡]Corresponding author. E-mail: ljq@aphy.iphy.ac.cn
© 2024 Chinese Physical Society and IOP Publishing Ltd

ics.

Besides the study of ultrafast dynamics, the UTEM has become an important platform in the study of electron–photon interactions since the proposal of a new technology called photon-induced near-field electron microscopy (PINEM).[15] The fast electrons of the UTEM can be inelastically scattered not only by the electrons confined in the material but also by the laser-excited near field in the nanomaterial or nanostructure. On this basis, PINEM is adopted for nanometer-scale near-field imaging. Meanwhile, the near-field scattering of free electrons suggests that electron wave packets can be shaped by controlling the intensity and spatiotemporal distribution of the near field. Interaction with the near field leads to the longitudinal bunching of the electron pulse and generation of an attosecond pulsed train after a distance of free drift.[16] Transverse modulation of the electron beam has also been carried out.

As a powerful tool for the study of ultrafast dynamics and free-electron–light interactions, the UTEM has the potential to provide new insights into the underlying physics of a wide range of phenomena in condensed matter physics, quantum mechanics, materials science, life sciences, and chemistry. This review introduces the use of the UTEM in studies on structural dynamics, phase transitions, electron dynamics, near-field imaging, and light shaping of the electron wave function.

2. Principle and instrumentation of the UTEM

The UTEM, used to detect dynamic processes at an atomic spatial resolution on the time scale of femtoseconds to nanoseconds, is realized by adopting the pump–probe method, combining an ultrafast laser and TEM.[17] As shown in Fig. 1(a), the optical pump beam from the ultrafast laser is focused onto the sample and initiates the dynamic process. Another ultraviolet probe beam from the same laser irradiates the photocathode inside the electron gun to generate pulsed electrons for detecting the transient process. By changing the time delay between the pump and probe pulses, it is possible to record the dynamical evolution of the sample through imaging, diffraction, and spectroscopy. Owing to the low dose of the pulsed photoelectron, millions of cycles are needed to accumulate a signal sufficient for data analysis.

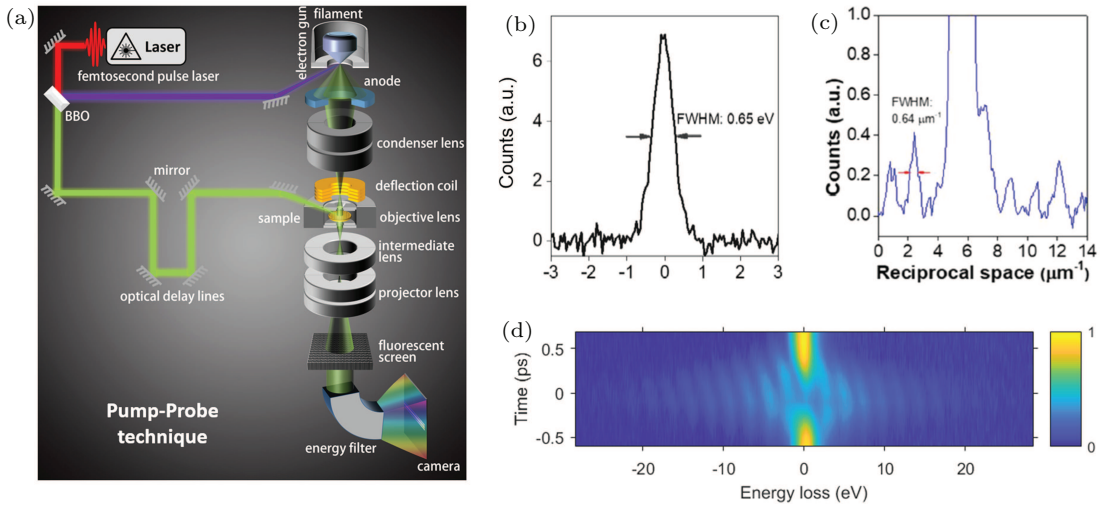


Fig. 1. Principle and relevant data of the UTEM. (a) Schematic of the UTEM based on the pump–probe technique; (b) energy resolution and (c) reciprocal resolution from the latest laser-driven Schottky field emission source (reprinted with permission from Ref. [18]); (d) electron pulse duration measured through photo-induced near-field microscopy.

The first-generation UTEM is based on a thermionic electron gun with a LaB_6 or Ta cathode having a size of tens of micrometers.[19–21] The so-called single-electron mode is adopted to eliminate pulse and energy broadening due to Coulomb repulsion inside a high-density pulsed electron bunch (i.e., the space-charge effect). To achieve a sufficiently strong signal in the high-magnification image mode within a reasonable exposure time, the electron number in one pulse is increased to 10^3 at the expense of temporal and energy resolution. A bias voltage is applied to a Wehnelt electrode[22,23] to balance the temporal and energy resolutions. The second-generation UTEM has a modified field emission electron gun for improved transverse coherence of the pulsed electron beam.[18,24–26] Several imaging methods that need high transverse coherence have been demonstrated; e.g., convergent-beam electron diffraction[27] and holography methods.[28] The latest UTEM has a nominal resolution of 200 fs, 0.2 nm, and 0.6 eV at a low single-pulse electron dose (i.e., 0.01 e^-/pulse). The extremely low single-pulse electron dose and high repetition rate limit the application of the UTEM, making it difficult for the UTEM to play a full role in the study of important processes, such as the multi-degree-of-freedom decoupling of strongly correlated systems and light-induced transient superconductivity. Recently, the laser-free UTEM[29,30] was proposed and demonstrated using a radio-frequency electric field to deflect and chop the contin-

uous electron beam and thus form a pulsed electron beam with a gigahertz repetition rate. However, the ultra-high repetition rate limits the scope of application to highly reversible processes with a recovery time of nanoseconds, which is only possible for electronic-related processes. The accelerator-based MeV ultrafast electron microscope[31,32] has been proposed as a promising tool for overcoming the space-charge effect in the study of structural dynamics at the nanometer spatial scale and the picosecond temporal scale, but the practical realization of MeV electron optics is challenging. Radio-frequency[33–35] or terahertz[36,37] pulse compression is another promising approach for overcoming the space-charge effect and increasing the usable single-pulse electron dose.

Another operation mode, the so-called single-shot mode or dynamic TEM (DTEM), where a single electron pulse contains more than millions of electrons to achieve enough electron dose required for one diffraction/image, can be adopted for capturing the irreversible process. DTEM has been extensively used for the study of thermal melting, crystallization[38] and phase transition process with the time resolution of tens of nanoseconds, which is limited by the intrinsic space charge effect of sub-relativistic electrons. We refer the interested reader to existing reviews[5,39,40] that cover the application of DETM which this review does not mention. With the development of MeV UTEM, the time resolution may be improved to picosecond level for studying irreversible process occurring on the non-thermal time scale.

3. Ultrafast structural dynamics and phase transitions revealed by ultrafast selected-area electron diffraction and real-space imaging

Ultrafast structural processes that occur following excitation can be visualized[41–43] and cross-checked[44] adopting both real-space (imaging) and reciprocal-space (diffraction) approaches for a UTEM, providing atomic and morphological information with femtosecond time resolution. Using ultrafast selected-area electron diffraction (USAED), one can get both the mean atomic displacements of short-range order following the Debye–Waller relation (i.e., the diffraction intensity change of the main Bragg peak) and the crystal lattice change of long-range order with precision of 10^{-4} nm (i.e., the position shift of the Bragg peak). Upon laser excitation of the TEM sample, energy is first transferred to the carriers (electrons or holes). The hot carriers then transfer energy to phonons through electron–phonon and phonon–phonon couplings, increasing the lattice temperature. The UTEM, sensitive to the change of lattice degree of freedom, can be used to study the microscopic electron–phonon coupling and phonon–phonon coupling processes as well as the macroscopic lattice expansion/contraction and coherent acoustic phonon generation processes in low-dimensional nanomaterials.[45] Taking one-dimensional multi-walled carbon nanotubes (MWCNTs) as an example,[21,46] USAED is utilized to track both the radial and axial responses of MWCNTs upon laser excitation of 45 mJ/cm^2 by monitoring the positional shift of the diffraction ring (Figs. 2(a)–2(b)). Nonthermal atomic motions in MWCNTs result in rapid intralayer expansions and interlayer contractions in the first several picoseconds, followed by lattice heating and thermal diffusion. The results demonstrate anisotropic, cooperative, and inverse collective atomic motions in intralayer and interlayer directions, illustrating the nature of the electron-driven nonthermal process and electron–phonon thermalization in low-dimensional nanomaterial. In addition, anisotropic lattice movements due to the difference between intralayer and interlayer bondings are observed in two-dimensional layered films,[47–50] such as transition-metal dichalcogenide 1T-TaSeTe.[51] Figure 2(c) shows the electron diffraction pattern taken along the [212] zone-axis direction, which is 25° from the surface normal. The intensity change of the (–120) in-plane Bragg spot after laser excitation of 7 mJ/cm^2 has a typically decreasing trend with an electron–phonon coupling time of 4.5 ps. The Bragg peak position along the (10–1) direction has oscillatory characteristics with a period of 48 ps, corresponding to a propagation time of the out-of-plane breathing mode (coherent acoustic phonon) of $T = 2L/v$, where $L = 60$ nm is the thickness of the sample and $v \approx 2500$ m/s is the sound velocity. Lattice expansion within the a–b plane is imperceptible. The large anisotropic lattice expansion leads to a complex diffraction intensity evolution of the Bragg spot with out-of-plane components, which can be analyzed considering the Debye–Waller effect, the initial deviation parameter, and multiple scattering.

While the USAED allows observation of atomic-scale lattice changes and coherent phonons, the information is typically from an averaged area of several square micrometers, depending on the size of the selected-area aperture. However, ultrafast real-space imaging can be adopted to directly visualize the morphological change in a range from nanometers to micrometers. So far, although atomically resolved real-space dynamic processes have not been reported,[53] the UTEM has played a key role in investigations of the generation, propagation, and evolution of coherent acoustic phonons (strain waves).[13,52,54,55] For example, Zhang *et al.*[52] examined a mechanically exfoliated van der Waals material, 2H-MoS_2, where two bend contours (labeled 1 and 2 in Fig. 2(e)) are separated by a crystal step edge. Owing to the different layer numbers, photo-induced coherent strain waves traveling back and forth across the layers possess different periods, leading to a gradual dephasing of the oscillatory signal between the two regions (Fig. 2(f)). This bright-field bend contour imaging is used to investigate the lateral propagation of acoustic phonons, anisotropic strain-wave dynamics, effect of discrete defects on acoustic phonons, and phase-velocity dispersion of hypersonic phonons.

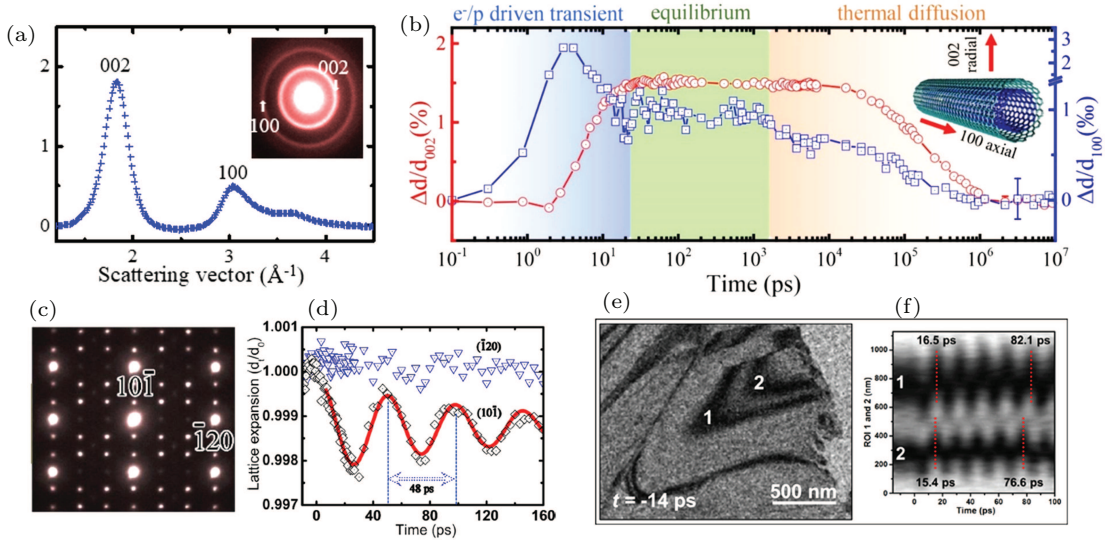


Fig. 2. Ultrafast structural dynamics and coherent acoustic phonons. (a) Transient one-dimensional electron diffraction profiles of multi-walled carbon nanotubes radially integrated from a two-dimensional diffraction pattern (inset) (reprinted with permission from Ref. [46]). (b) Temporal phase diagram of the reversible structural evolution of photoexcited multi-walled carbon nanotubes for a fluence of 45 mJ/cm^2. The lattice response in the radial and axial directions shows anisotropic multi-staged processes, including electron/phonon-driven transience, equilibrium heating, and thermal diffusion (reprinted with permission from Ref. [46]). (c) Electron diffraction pattern slightly off the [212] zone-axis direction in 1T-TaSeTe (reprinted with permission from Ref. [51]). (d) Temporal evolution of the Bragg peak position shown in (c) excited by a femtosecond laser with fluence of 7 mJ/cm^2 (reprinted with permission from Ref. [51]). (e) Bright-field electron micrograph of MoS_2 thin film featuring two bend contours that are separated by a crystal step edge, imaged at 14 ps prior to photoexcitation (reprinted with permission from Ref. [52]). (f) Space–time contour plot of the intensity modulation for the two bend contours in (e), where the first and the fifth periods are marked by vertical lines, showing few-layer dephasing of photo-induced strain waves (reprinted with permission from Ref. [52]).

In addition to the examination of strain waves using the dynamic movement of bend contours, the UTEM plays a powerful role in the domain-related photo-induced phase transition, such as the domain melting, nucleation, and growth. The charge-density wave (CDW) phase transition has been widely investigated by adopting the ultrafast electron diffraction (UED)[56–60] and the UTEM.[61–64] Through photoexcitation, an optically induced CDW transition in 1T-$TaSe_2$ from the commensurate (C) phase to the incommensurate (IC) phase has been captured utilizing USAED in UTEM investigations,[62] where the transition is characterized by changes of the satellite peak position and intensity as shown in Fig. 3(a). The UTEM has also been used to characterize the structure of the laser-induced hidden state. In 2014, Stojchevska *et al.*[65] demonstrated that a single 1–3 mJ/cm^2, 800-nm femtosecond light pulse could convert the low-temperature insulating state of 1T-TaS_2 into a hidden (H) metastable metal, which could be driven back into an insulator adopting picosecond pulse trains or heating. *In-situ* cooling transmission electron microscopy observations[63] revealed a clear transition from a commensurate CDW phase (q_C) to a new CDW order with $q_H = (1-\delta)q_C$, as indicated by the change of satellite peak position in Fig. 3(b). Subsequent H-CDW domain relaxation yielded a stable metallic phase under a high-fluence excitation (5 mJ/cm^2). The simulated diffraction pattern of the polaron-ordered structural model with CDW domains was consistent with observations, indicating that the defect-related domain wall is the key to the stable and reversible control of the hidden state. Ultrafast dark-field electron imaging[64] was used to map the order parameter across a laser-induced phase transition in 1T-TaS_2 from the near C phase to the IC phase (Fig. 3(c)). A tailored dark-field aperture array was inserted on the focal plane of the objective lens to track the evolution of CDW domains with simultaneous femtosecond temporal and 5-nm spatial resolution, revealing relaxation pathways and domain wall dynamics. The initial suppression pattern and the shape of the CDW domain were consistent with the spatial profile of the excitation density.

The structural phase transition has been extensively studied adopting the UED[68–70] and the UTEM.[66,71,72] Zhang *et al.*[66] examined the photo-induced martensitic (MT) transition and reverse transition in a shape memory alloy $Mn_{50}Ni_{40}Sn_{10}$ through ultrafast bright-field imaging. The series of ultrafast micrographs in Fig. 3(d) show the periodic annihilation and creation of domains with a laser-pumping fluence of 10 mJ/cm^2. The period ($\sim$ 40 ps) is consistent with the propagation time of the round-trip breathing oscillation, indicating strong coupling between the MT transition and lattice breathing mode. A more careful analysis of the ultrafast images and the corresponding electron diffraction patterns shows remarkable transient states, namely, the MT nucleation with a coherent twinning nature, the constraint of *C*4 symmetry on the growth of the MT nuclei, and the rapid growth of MT plates. These results highlight the ability of the UTEM to directly probe the collective atomic motion related to symmetric breaking and to clarify the mechanisms of domain wall nucleation in multifunctional materials.

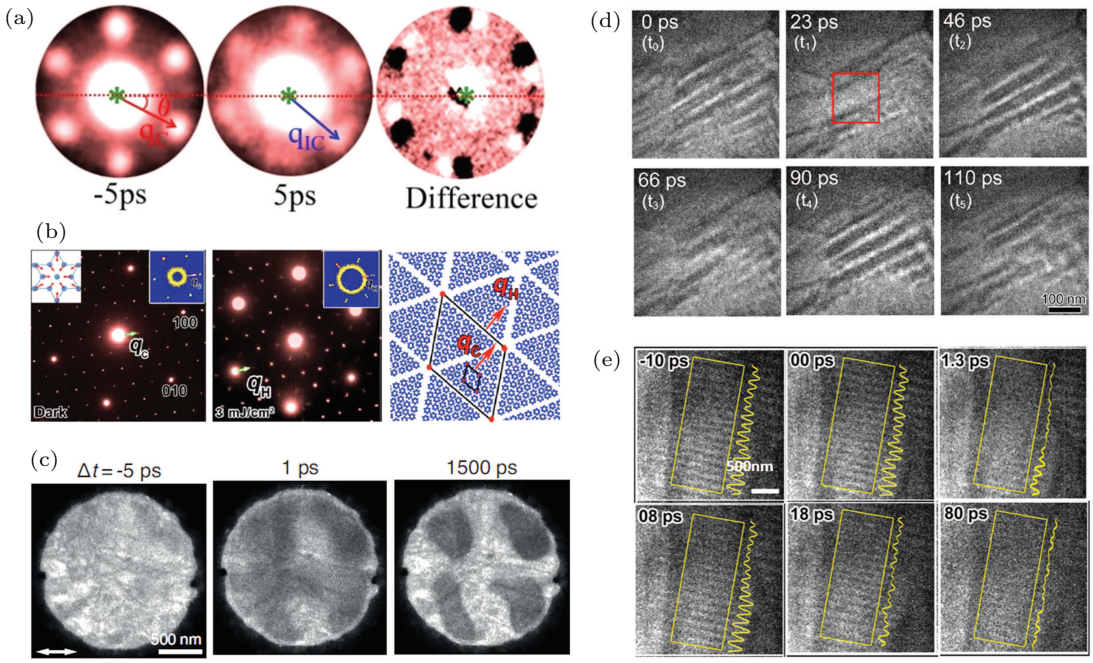


Fig. 3. Photo-induced phase transition by ultrafast electron diffraction and microscopy. (a) Optically induced charge-density wave phase transition in 1T-$TaSe_2$ revealed by the satellite peak change in diffraction pattern (reprinted with permission from Ref. [62]); (b) hidden state in 1T-TaS_2 induced by a single ultrafast laser pulse (reprinted with permission from Ref. [63]); (c) laser-induced charge-density wave phase transition in 1T-TaS_2 captured by dark-field imaging (reprinted with permission from Ref. [64]); (d) martensitic transition and nucleation in the shape memory alloy MnNiSn detected by bright-filed imaging (reprinted with permission from Ref. [66]); (e) magnetic dynamic transition in Mn–Ni–Ga obtained by ultrafast Lorentz microscopy (reprinted with permission from Ref. [67]).

The magnetic dynamic phase transition can be studied through ultrafast Lorentz microscopy.[73–75] Zhang *et al.*,[67] for example, reported photo-induced ultrafast magnetization dynamics in Mn–Ni–Ga. Three successive dynamic processes involving four distinct magnetic states were observed. As shown in Fig. 3(e), upon optical excitation, the magnetic contrast of Mn–Ni–Ga was first suppressed at approximately 1 ps, then rapidly recovered within a few picoseconds, and was finally suppressed fully at $\sim$ 80 ps. After photoexcitation, the electrons almost instantaneously acquired photonic energies within tens of femtoseconds and the hot electrons rapidly transferred their excess energy to the spins within hundreds of femtoseconds, resulting in the ultrafast destruction of spin angular momentum. As the electron spin subsystem thermalized the lattices on a picosecond time scale, there was a partial recovery of magnetization. Further thermalization of the electron–spin–lattice subsystems reached a new thermally equilibrated state at an elevated temperature, at which the magnetization was suppressed or even destroyed above T_C. The results demonstrate the feasibility of directly imaging ultrafast demagnetization in real space and relevant dynamic behaviors in complex spin textures with a nanometer–picosecond spatiotemporal resolution through ultrafast Lorentz microscopy.

4. Electronic dynamics traced through time-resolved EELS

Dynamic multimodal probing of the lattice and electron system in advanced materials is a promising way to disentangle degrees of freedom whose coupling leads to exotic equilibrium and transient properties.[76–78] Besides the techniques developed for the characterization of structural dynamics described above, the intrinsic electronic dynamics of materials can also be uncovered using the versatile UTEM. EELS is a sophisticated technique which records the energy distribution of electrons that have passed through the specimen. Tremendous information about the electron system, such as the band gap, dielectric response, bonding/valence state, and nearest-neighbor atomic structure, can be extracted from the signals arising from inelastic scattering processes.[79] When combined with the time-resolving capability of the UTEM, the electronic dynamics can be traced with different temporal resolutions, depending on the energy-loss region detected.

The so-called low-loss region normally ranges 0–50 eV. The characteristic peaks of low-energy elementary excitations, such as the phonon and exciton, are swallowed in the zero-loss peak and undetectable, even with the best ever achieved energy resolution (0.63 eV, determined from the full width at half maximum of the zero-loss peak)[80] of the UTEM. The resonant oscillation of the electron gas (plasmon) and electron transition from the shallower core levels to empty states contribute the main features in this region. Time-resolved low-loss EELS has been adopted to reveal the electronic dynamics in graphite,[81,82] layered manganite,[83] and single-wall carbon nanotubes.[84] Considering the picosecond time scale investigated in these studies, the dynamics of chemical bonding and orbital charge are closely related to the photon-induced

transient structural transformations in the materials.

In the case of graphite, a distorted stacking of the layers along the *c*-axis due to strong coherent in-plane vibrations can lead to lattice contraction, followed by expansion and recurrences.[81] The chemical bonding of carbon atoms can thus be affected. During the interaction of incident electrons with the specimen, the collective dynamics of valence electrons are excited and the change in plasmonic properties of bonding carriers is reflected by the intensity variation and position shift of plasmon peaks in EELS, as shown in Fig. 4(a). A π phase shift between the time-dependent intensity variations of the surface plasmon peak and bulk plasmon peak is identified and accompanied by the blueshift and later redshift of the bulk plasmon peak. With the aid of *ab-initio* calculations, these dynamic features are attributed to the reciprocating switching between the diamond-like and graphene-like charge-density distributions in photoexcited graphite.[82]

The similar technique has been used to uncover the dynamics in one-dimensional materials, such as single-wall carbon nanotubes, in which electron-driven and phonon-driven lattice expansions on different time scales are distinguished.[84] To clarify the origin of a 0.18% lattice expansion with a time constant of 1.4 ps and lattice expansion of 0.15% with a time constant of 17.4 ps measured from ultrafast electron diffraction, the dynamics of the π plasmon and $\pi+\sigma$ plasmon were investigated by Zheng *et al.*, as presented in Figs. 4(b)–4(e). The redshifts of surface and bulk plasmon peaks in EELS are maximized at a time delay of ~ 1 ps and followed by long-lived and partial recovering (see Figs. 4(c) and 4(d)). According to the Drude model, the shifts toward lower plasmon resonance energy are attributed to a decrease in the valence electron density, mainly resulting from the laser-promoted electron transfer from the valence band (π) to the conduction band (π^*). The weakened chemical bonding gives rise to the fast lattice expansion. Afterwards, there is energy transfer from the electron system into lattice vibration, accompanied by an intensity decrease of the $\pi+\sigma$ plasmon (Fig. 4(e)).[84]

In addition to the change of plasmon, the changes of low-energy ionization edges reflect rich electronic dynamics. In $PrSr_{0.2}Ca_{1.8}Mn_2O_7$, an electron strong correlation system, the characteristic shallower core levels of Pr $O_{2,3}$, Sr $N_{2,3}$, Ca $M_{2,3}$, and Mn $M_{2,3}$ are presented in the low-loss region.[83] When a relatively intense laser irradiates the specimen, the heat can drive the system from a charge/orbital ordering state into a metallic state, and the pressure wave generated by the temperature jump provokes coherent structural motions with a period of tens of picoseconds. Owing to the strong coupling between the lattice and electron, the consequent oscillation of the electron system can be monitored through ultrafast EELS. The time-dependent intensity variations are different from each other for the four elements and two plasmons, as shown in Fig. 4(f), reflecting different sensitivity to the structural change. Especially for Mn, the large crystal field results in the clearest periodicity.

The changes of the high-loss portion of the spectrum above ~ 50 eV, namely, the ultrafast core-loss EELS, provide complementary electronic dynamic information of materials.[14,85–87] This energy region is characterized by excitations of core-level electrons into unoccupied higher lying states of the crystal or even to a free-electron state, providing information on the local geometric structure and chemical bonding, which is similar to that provided by x-ray absorption spectroscopy. The overall signal intensity drops rapidly with increasing energy loss, and the element-specific core excitations are superimposed on a smoothly decaying background, leading to difficulties in acquiring data with a sufficient signal-to-noise ratio. Thus, a much longer acquisition time, timely energy drift correction, and high-performance electron detection camera should be considered.[85] The core-loss signal has the ability to fingerprint different forms of the element, especially for carbon and 3d transition metals, making it an efficient tool for tracking the dynamics of chemical bonding and valence state.

The photo-induced lattice contraction and expansion in graphite studied through time-resolved low-loss EELS[81] were further investigated in the core-loss region with nanosecond and picosecond resolutions, as shown in Fig. 4(g).[85] Owing to the high sensitivity of the σ^* edge onset to the carbon–carbon bond length in the *a*–*b* plane, the redshift on a nanosecond time scale reflects the elongation of the in-plane bond length and the existence of thermal disorder at high temperatures. In addition, the picosecond redshift was attributed to the downward shift of the empty σ^*-band and thus shrinkage of the band gap. Meanwhile, the change in the oxidation state of Fe in a photocatalyst α-Fe_2O_3 was explored after laser excitation. The broadening of the Fe L_3-edge (with energy loss of approximately 709.5 eV) occurring within a few picoseconds was believed to originate from the charge transition from (Fe^{3+}–Fe^{3+}) to (Fe^{2+}–Fe^{4+}).[14]

It is noted that the PINEM signal inevitably exists in both ultrafast low-loss and core-loss spectroscopy, leading to the broadening of all features within approximately -1 to 1 ps.[14,83,85,87] The dynamics of intrinsic electronic properties, such as chemical bonding and the valence state, should be treated with extreme caution. The deconvolution operation might be an optional method for eliminating this effect.[14] Nevertheless, the time-resolved PINEM technique has been successfully applied to trace the phase transition and plasmon-enhanced structural dynamics in low-dimensional

materials.[88–90] Adopting the so-called PINEM-gating technique (see the next section) and the recently developed two-color PINEM method, the electronic dynamics during the insulator–metal phase transition in VO_2 can be followed with much improved temporal resolution owing to the high sensitivity of PINEM to the dielectric response (Fig. 4(h)).[88,89] Moreover, Zheng *et al.* found that the photon-induced lattice contraction in a multi-walled carbon nanotube can be enhanced under the effect of the azimuthal surface plasmon, by combining the PINEM and ultrafast electron diffraction measurements. When the light polarization is perpendicular to the tubular axis, the excited azimuthal plasmon modulates the charge distribution and gives rise to a notable Coulomb force that compresses the lattice. The time-dependent PINEM signal and the lattice contraction thus exist on a consistent time scale.[90]

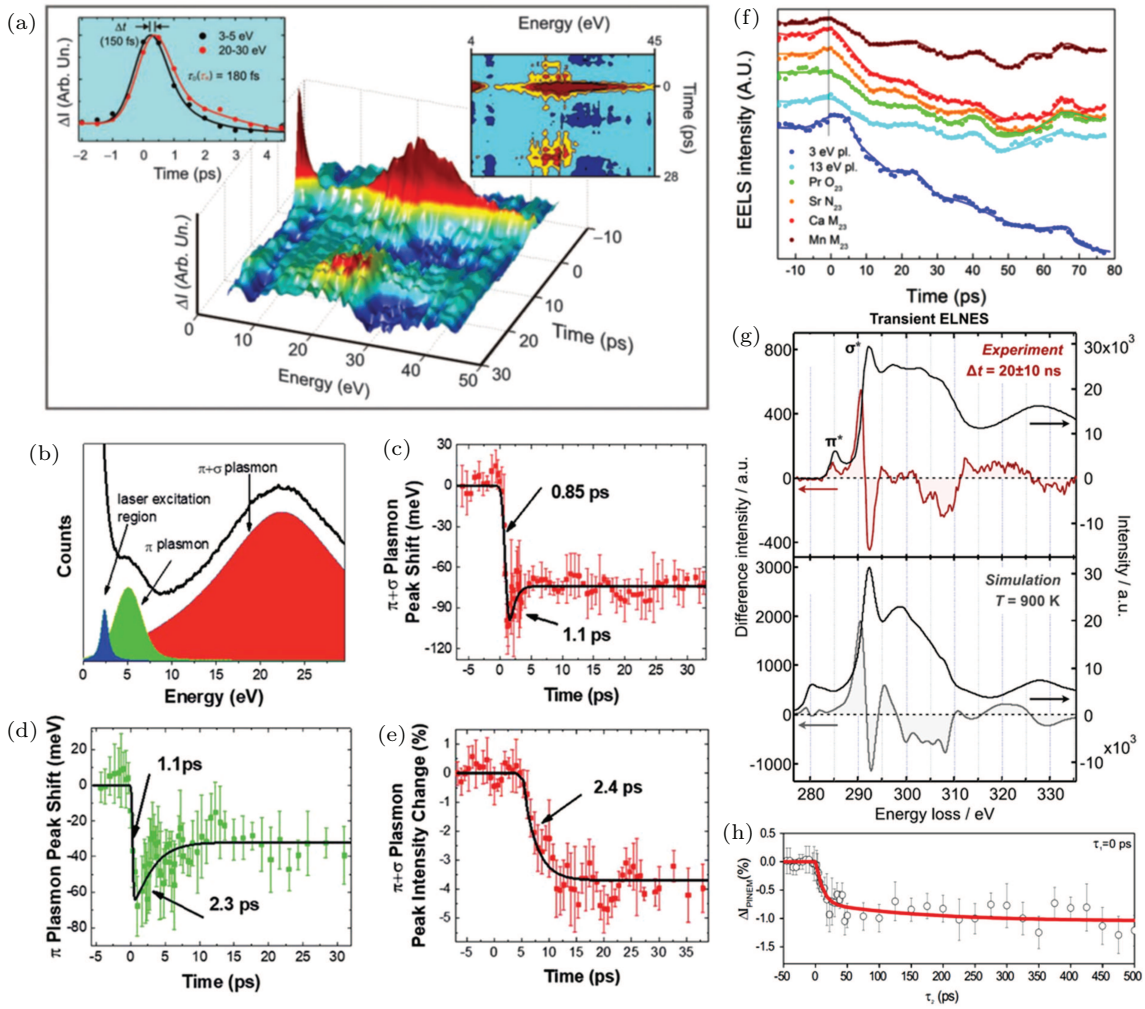


Fig. 4. Electronic dynamics traced through the UTEM. (a) Three-dimensional intensity–energy–time EELS plot for graphite. The plot shows the time–energy–amplitude evolution of spectral changes at different time delays. The inset on the left depicts two transients for the band at the laser energy (3–5 eV) and that of the bulk plasmon (26.9 eV) (reprinted with permission from Ref. [81]). (b) Static EELS profile of single-walled carbon nanotubes (black line). The red region (band located at ~ 22.4 eV) represents $\pi+\sigma$ plasmons. The green region (band located at ~ 5 eV) represents π plasmons (reprinted with permission from Ref. [84]). (c) Time dependence of the $\pi+\sigma$ plasmon peak energy shift after laser excitation of 44 mJ/cm^2 (reprinted with permission from Ref. [84]). (d) Time dependence of the π plasmon peak energy shift (reprinted with permission from Ref. [84]). (e) $\pi+\sigma$ plasmon peak intensity change, showing a 3.5% decrease in amplitude and a time constant of 2.4 ps (reprinted with permission from Ref. [84]). (f) Temporal profile of the EELS intensity at selected energies, in correspondence with the specified electron states in $PrSr_{0.2}Ca_{1.8}Mn_2O_7$ single crystalline nanoparticles (reprinted with permission from Ref. [83]). (g) Nanosecond-resolved core-loss spectroscopy for graphite. Upper panel: experimental static ($< t_0$) and transient K-edge energy-loss near-edge spectroscopy at $\Delta t = 20 \pm 10$ ns after laser excitation at 532 nm; lower panel: theoretical static and transient energy-loss near-edge spectroscopy based on molecular dynamics simulations at room temperature and 900 K (reprinted with permission from Ref. [85]). (h) Phase transition in vanadium dioxide nanoparticles. The change of the PINEM spectrum intensity, obtained from the coupling between the first optical and electron pulses on the nanoparticles, as a function of the second optical pulse (pump) delay (reprinted with permission from Ref. [88]).

Although various time-resolved EELS techniques have been developed, their capabilities are still not on par with those of well-developed ultrafast spectroscopy, newly developed time-resolved angle-resolved photoemission spectroscopy and time-resolved scanning tunneling microscopy in exploring the electronic dynamics of condensed matter. However, with the continuous optimization of the UTEM, electron pulses with high brightness, high coherence, and short duration width are expected. New techniques offering high performance, such as time-momentum-resolved EELS, ultrafast convergent-beam

electron diffraction, and time-resolved four-dimensional scanning transmission electron microscopy, are thus expected to be realized and provide more insight into the dynamics of electrons and coupling with other degrees of freedom.

5. Imaging the near-field distribution with the UTEM

As an important technique developed with the UTEM, PINEM is an emerging method of studying the near-field mediated electron–photon interaction, especially in near-field imaging. The first experimental results of PINEM were reported by Zewail and co-workers in 2009.[91] This pioneering work reported the EELS spectra of carbon nanotubes illuminated by an intense femtosecond laser pulse. As the pulsed electron pockets pass through the confined near field at the nanostructure, they lose or gain integer multiples of the photon energy and show a series of discrete peaks in EELS (Fig. 5(a)). In addition, the photon-excited evanescent field distribution has been directly imaged with nanometer resolution in the energy-filtered transmission electron microscopy (EFTEM) mode, using an energy filter to select only electrons that have absorbed or emitted photons to form an image.

Theoretical methods for PINEM analysis have been developed on the basis of Green's function formalism,[92] the direct integration of the time-dependent Schrodinger equation,[15] and a ladder operator formalism.[16] Both Green's function formalism and the direct integration of the time-dependent Schrodinger equation consider the time evolution of the wave function of a subrelativistic electron traveling through the classical electromagnetic wave, whereas the ladder operator formalism gives a quantum description of electrons scattered by coherent photons in the second quantization and predicts the multilevel Rabi oscillation in populations of electron momentum states. This prediction has been clearly demonstrated in EELS measurements of electrons inelastically scattered by a uniform near field,[16] paving the way for theoretical studies of free-electron quantum optics.

In the PINEM regime, the free-electron–photon interaction occurs via the linear coupling between electron and optical fields. The electron–photon coupling strength is quantified by the factor β,[15,16,92]

$$\beta(x,y) = \frac{e}{2\hbar\omega}\int_{-\infty}^{+\infty} E_z(x,y,z)\,\mathrm{e}^{-\mathrm{i}(\omega/v_\mathrm{e})z}\mathrm{d}z, \tag{1}$$

where $\hbar$ is the reduced Plank constant, E_z is the electric field component along the propagating direction of the electron pulses, ω is the angular frequency of photons, and v_e is the relativistic group velocity of the electron packet. The population of the nth EELS sideband at position (x,y) is given by

$$P_n(x,y) = J_n^2\left(2\left|\beta(x,y)\right|\right), \tag{2}$$

where J_n denotes the nth-order Bessel functions of the first kind. As the coupling strength is the spatial integral of the near field of the z-component, the spatial and temporal distributions of the near field are imprinted in the spatially dependent EELS sidebands, providing a powerful technique for the imaging of the spatiotemporal dynamics of plasmonic near fields with high spatial and temporal resolutions.

The energy and time resolutions are crucial to the dynamic characterization of the non-equilibrium process. In PINEM observations, the energy resolution depends on the spectral bandwidth of the pump laser rather than on the electron spectrometer, allowing surface plasmon polariton (SPP) modes to be probed with meV spectral resolution. By combining the narrow bandwidth optical pulse with an optical parameter amplifier, the spatial mapping of plasmon modes in a silver nanowire has been achieved with energy resolution of 20 meV (Fig. 5(b)).[93]

Limited by the electron pulse duration, the temporal resolution of PINEM is on the order of hundreds of femtoseconds. The PINEM-gating technique, which is based on the electron interaction with two optical pulses, improves the temporal resolution to the order of tens of femtoseconds.[80,88] The delay of the first pulse (gating pulse) relative to the electron pulse is kept at $t = 0$ to generate the gated electron pulse with maximum counts. The duration of the gated electron depends on the duration of the gating pulse. The time delay of the second pulse, which initiates the non-equilibrium process, can be scanned across the gated electrons to characterize the process. The time resolution of the PINEM-gating technique depends on the time duration of the gating pulse rather than on that of the original electron pulse (Fig. 5(c)), allowing for better time resolution when using a short gating pulse. The PINEM-gating technique has been theoretically generalized to the attosecond regime and is expected to produce isolated attosecond electron pulses.[94]

As a powerful tool for studying the electron–photon interaction at the nanometer scale, PINEM has been used to image the surface plasmons, including the localized surface plasmon resonance (LSPR) and SPPs, of nanoparticles,[95–97] nanotips,[16] metallic nanowires,[98] carbon nanotubes,[90,91] rough metallic films,[99] and biological structures.[100] A new and typical application of PINEM for imaging plasmonic near fields is on an asymmetric bowtie nanostructure.[101] The bowtie nanostructure, a typical surface plasmon field enhancement device, has important applications in optical sensing and surface-enhanced Raman scattering. PINEM performed using a UTEM provides the plasmonic near-field excitation characteristics of the laterally illuminated bowtie nanostructure with different polarizations of the incident laser. A chiral SPP standing wave was observed on tips with polarization parallel to the bowtie axis, whereas LSPR oscilla-

tions were observed with perpendicular polarization excitation (Fig. 5(d)). The excitation lifetime was analyzed by combining the time-dependent PINEM theory with spatiotemporally resolved PINEM images, demonstrating that the lifetime of SPPs is longer than that of LSPR.

Previous imaging techniques have mainly focused on imaging SPP standing waves because the observation of a traveling SPP is restrained by the time resolution. PINEM, based on the coherent electron–photon interaction, enables characterization of the traveling SPP, which is similar to holographic imaging.[102] The reference field can be a second SPP excited by another independent pulse or an optical field with a homogeneous plane-phase distribution generated by an illuminated thin film. When the electrons are inelastically scattered by the signal SPP and the reference field in turn, the spatial distribution of the coupling strength depends on the relative phase between the signal field and reference field. The holographic PINEM image can be generated by selecting the elastic scattering electrons to form an EFTEM image (Fig. 5(e)). The phase velocity of the SPP and the group velocity of the wave packet can be extracted from the holographic PINEM image. As a TEM-based approach, holographic PINEM enables the imaging of plasmonic fields at the buried interface, which is different from the conventional application of imaging plasmonic near fields outside the material.[103]

Another unique application of PINEM is the direct imaging of the nonlinear features of SPPs[104] in what is called single-photon order-selected electron imaging (SPOSEI).[105] SPOSEI is an EFTEM image formed by the electrons selected within the single-photon energy window, allowing characterization of the near fields associated with the absorption of a specific number of photon quanta. Appropriate sidebands should be selected for imaging to improve the contrast and quality of the image. For a silver nanowire illuminated by a pump laser with high power density and parallel polarization, the EFTEM formed by the electrons absorbing two to five photons revealed plasmon oscillations with a mix of a major long period and minor short period at the laser-facing surface. The major mode was the excited SPP with the fundamental frequency, whereas the minor mode was attributed to the second-harmonic generation near fields (Fig. 5(f)).

In addition to the SPP and LSPR, PINEM can be applied to microcavities and photonic crystals.[106,107] The UTEM provides a flexible experimental setup, allowing the characterization of a photonic crystal in the real space and energy space. By changing the polarization, incident angle, and wavelength of the pump laser, the strength of electron–photon coupling can be varied and the band structure of the photonic crystal is reconstructed.

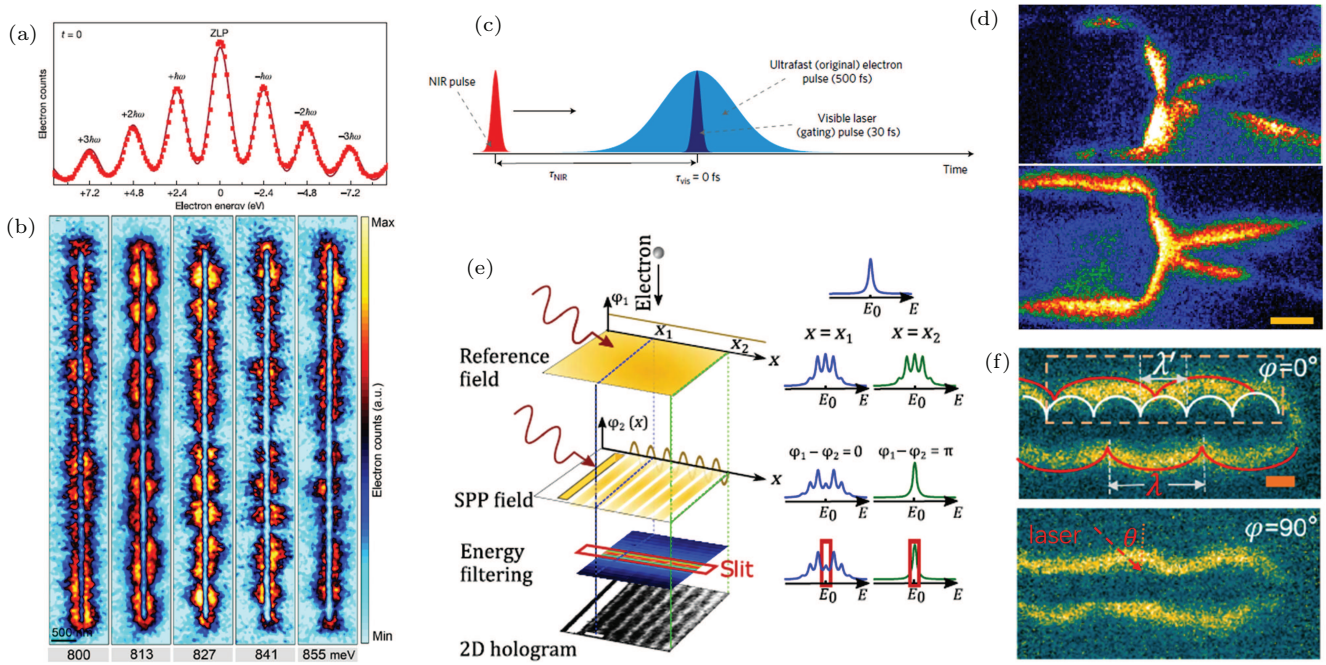


Fig. 5. Characterization of the near-field in energy and real space. (a) Example of EELS after the electron–photon interaction (reprinted with permission from Ref. [91]). (b) Series of PINEM images of a silver nanowire excited by a narrowband pump laser as a function of the wavelength of the photoexciting laser (reprinted with permission from Ref. [93]). (c) Schematic illustration of the PINEM-gating technique (reprinted with permission from Ref. [94]). (d) PINEM images of the asymmetric bowtie nanostructure under the polarization of a laser parallel (upper panel) and perpendicular (lower panel) to the bowtie axis. The upper panel shows asymmetric features whereas the lower panel shows symmetric features. The scale bar is 200 nm (reprinted with permission from Ref. [101]). (e) Principle of spatially separated electron holography. The reference field is a homogeneous optical field with a plane-phase distribution. The coupling strength depends on the relative phase between the SPP and reference field, which results in a position-dependent electron energy distribution. The hologram is formed with the zero-loss peak in EELS (reprinted with permission from Ref. [102]). (f) Partial photon order-selected electron images of a silver nanowire for an incidence angle $\theta = 24°$ and power density of 4.8×10^{10} W/cm^2. The short-period mode is observed on the front surface with parallel polarization (upper panel) but disappears with perpendicular polarization (lower panel) (reprinted with permission from Ref. [105]).

Beyond the conventional PINEM, which images the near fields of nanostructures under visible or infrared laser excitation, several studies have explored the imaging capability of the inelastic free-electron–photon interaction. For example, the evolution of electron clouds generated by high-flux pump lasers illuminating metallic structures and semiconductors has been studied in space and time, considering the interaction of free electrons with the terahertz near fields generated by a moving charge.[108,109] In addition to the SPP and LSPR, PINEM is expected to characterize other quasiparticles. So far, the wave packet dynamics of phonon–polariton excitations in two-dimensional materials have been studied with a mid-infrared laser pump.[110] Far-infrared laser and terahertz light sources are expected to be used for the UTEM, enabling characterization of the dynamics of more quasiparticles, including exciton polaritons and Cooper pair plasmon polaritons.

6. Shaping electron wave packets with light

As discussed above, PINEM based on the inelastic electron–photon interaction can imprint information about the electromagnetic field distribution on the electron wave function. The electron wave function can thus be manipulated by the designed electromagnetic field. The electron wave function after interaction is given by[111]

$$\phi(\boldsymbol{r},t)=\phi_0(\boldsymbol{r}-\boldsymbol{v}t)\,\mathrm{e}^{-2\mathrm{i}|\beta|\sin\left(\frac{\omega z}{v}+\arg(\beta)-\omega t\right)}, \tag{3}$$

where $\boldsymbol{v}$ is the electron velocity and $\phi_0(\boldsymbol{r}-\boldsymbol{v}t)$ is the electron wave function before interaction with the optical field. The electron wave function after the interaction is sinusoidally modulated in phase, enabling manipulation of both longitudinal and transverse components by the electromagnetic field. Phase-space manipulation in the longitudinal direction has been adopted for attosecond electron pulse trains[112,113] and electron acceleration,[114] and in the transverse direction for electron wavefront shaping.[115,116]

The classical view is that the longitudinal phase modulation is based on the tailoring of the electron wave function in the time domain.[117] The time-varying electromagnetic field modifies the electron wave packet, affecting the parts of the wave packet differently in the negative and positive electric fields, broadening the energy spread, and changing the spatial distribution of the wave packet in the longitudinal direction. For example, the electromagnetic field in the microwave range can compress the single-electron pulses of the UTEM under reasonable synchronization.[118] In the PINEM regime, as the visible or infrared laser used for pumping has a period shorter than the duration of the electron wave packet,[119,120] the wave packet is divided into accelerating and decelerating parts with the period of the light wave. During free propagation after the interaction, the accelerated parts catch up with the decelerated parts, resulting in a bunching of the electron density after a certain time.[16,121]

The concept of longitude phase modulation in PINEM was first mentioned and developed by Ropers and co-workers. The electron density in momentum space is reshaped by the period phase modulation of the electron wave function and the sideband orders acquire different phases during the propagation, shearing the phase-space distribution and forming attosecond electron pulse trains with a period equal to the optical period. In the case of electron energy of 200 keV for the UTEM, the propagation length is a few millimeters. In experiments, electron pulse trains with a peak duration of 655 as have been confirmed by reconstructing the Wigner function of the electron pulse after propagation (Fig. 6(a)), and a narrower peak duration could be realized with strong electron–photon coupling.[106,107,112,122] Pioneering experiments using attosecond electron pulse trains have been carried out, demonstrating potential application in imaging and diffraction.[123]

In addition to attosecond electron pulse trains, the phase control of the free-electron wave function has been investigated. An effective approach is to make the free electrons interact sequentially with two phase-locked near fields. In experiments,[111] two gold paddles were used to create two near fields separated by a distance of 5 μm. As the two near fields were spatially separated, the final wave function after the first interaction acted as an initial wave function for the second interaction. Each of the two interactions imposed a sinusoidal phase modulation on the electron wave function, and the total effect was the sum of the two modulations. This can be characterized by EELS, where the enhancement or cancellation of the coupling depends on the relative phase of the two near fields (Fig. 6(b)). In addition to the spatially separated near fields excited by a pump laser, two temporally separated electromagnetic fields have a similar effect, providing a simpler approach to controlling the longitudinal phase of the electron wave function.[124] In addition, asymmetric spectra generated by two temporally separated laser beams of frequencies ω and 2ω have been observed.[121]

Besides longitudinal phase modulation, transverse phase modulation has attracted much attention in recent years. The simplest transverse phase modulator is a membrane that is opaque or partially transparent to the incident laser light. Such a membrane creates a semi-infinite space to spread the momentum of photons, where some of the photons satisfy the energy–momentum conservation. In this state, the free electrons are scattered directly by the light waves rather than by the near fields excited by the pump laser, resulting in an angular deflection of the electron beams.[36,123–125] Unlike the Kapitza–Dirac effect,[126–128] where the free electrons are diffracted by a standing light wave, the scattering of free electrons by a semi-infinite light field is an inelastic process. The

transverse momentum exchange is accompanied by an energy exchange, and the direction and magnitude of the transverse momentum exchange depend on the geometric details. Taking advantage of the high coherence electron beam emitted from the Schottky field emitter tip, the quantized energy and transverse momentum transfer can be characterized in reciprocal space (Fig. 6(c)).[129] Using high-coherence free electrons and a uniform electric field, high-purity free-electron energy–momentum states can be realized, providing an elementary component for optically programmable electron phase plates.

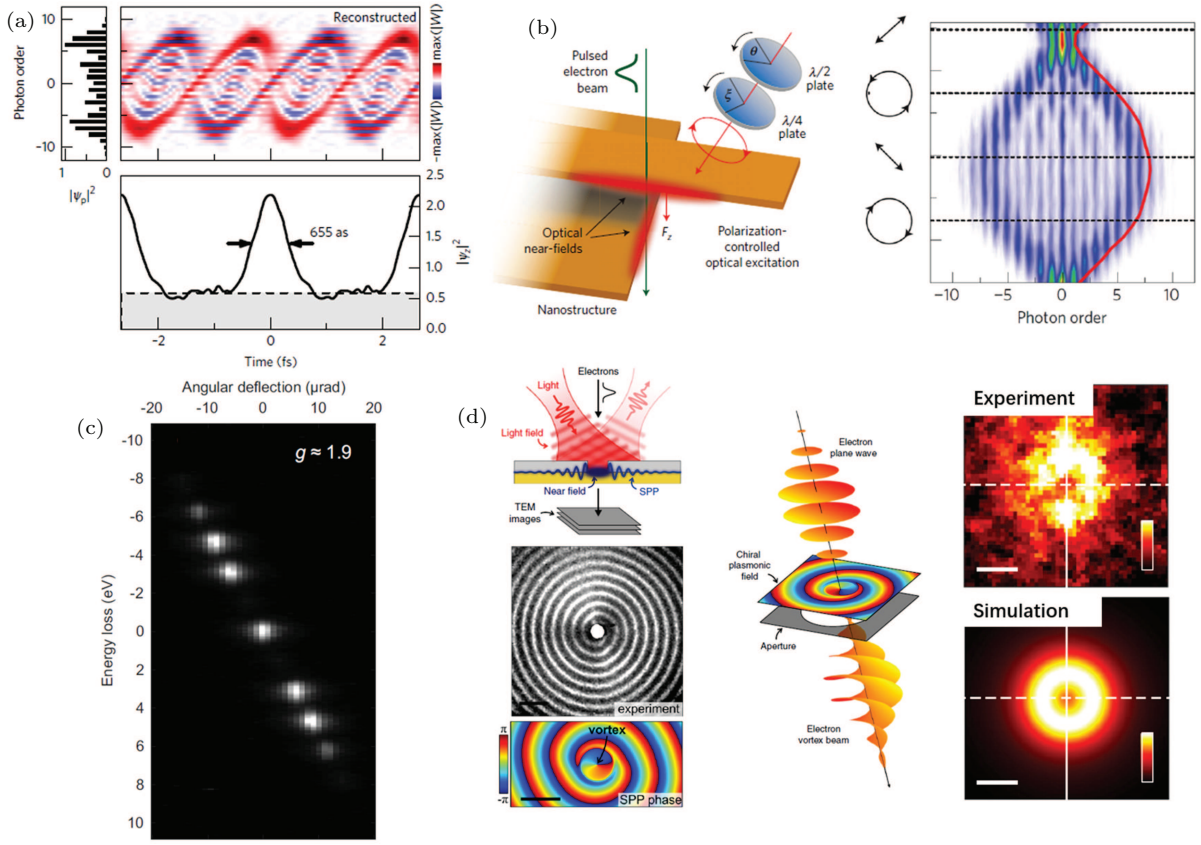


Fig. 6. Shaping of electron wave packets in longitudinal and transverse directions. (a) Reconstructed Wigner function of the propagated single-electron wave packet after interaction. The distance of propagation is 1.5 mm. Pronounced shearing due to free-space propagation is observed. The energy integral of the Wigner function shows a peak duration of 655 as (reprinted with permission from Ref. [121]). (b) Modulation of the electron wave function by spatially separated near fields. The electrons pass through the corner of two gold paddles, such that the electron wave function is modulated by two near fields (left panel). The right panel shows the EELS spectrum depending on the relative phase of the two near fields, which is controlled by the orientation of the $\lambda/2$ waveplate (reprinted with permission from Ref. [111]). (c) Transverse momentum distribution after interaction showing the quantized nature of the electron–photon coupling mediated by the membrane (reprinted with permission from Ref. [129]). (d) Generation of electron vortices by chiral plasmonic near fields. The left panel shows the two-dimensional hologram after the interaction, revealing a spiral phase pattern typical of a chiral plasmon. The middle panel shows the transfer of orbital angular momentum to electrons. The transfer of orbital angular momentum can be characterized in the reciprocal space (right panel) (reprinted with permission from Ref. [130]).

In addition to the plate medium, structures supporting SPPs have demonstrated the ability to manipulate the transverse electron phase. A typical and important nanostructure is an Ag/Si_3N_4 bilayer thin film with a nanocavity, which supports well-defined chiral SPPs under circularly polarized laser excitation.[130] Both the semi-infinite light field and SPPs interact with electrons, coherently manipulating the transverse phase and generating electrons with a well-defined orbital angular momentum. Unlike electron vortex beams generated by passive phase plates,[131–133] the electron vortex beam is generated by the exchange of orbital angular momentum between interacting relativistic electrons and chiral SPPs (Fig. 6(d)). Importantly, the ability to manipulate SPP fields enables the control of properties of the vortex beam with attosecond precision, which is beneficial for applications in non-equilibrium dynamics. Later research has used more patterns fabricated on the bilayer film, shown more types of spatially modulated free electrons[115,134,135] and verified that energy post-selection provides another method of controlling the transverse electron phase. Beyond the nanostructures, transverse electron phase modulation can be achieved using shaped light beams.[136,137]

Research on the quantum properties of the electron–photon interaction has advanced rapidly in recent years. In 2019, Kifr proposed Q-PINEM theory, which is a quantum-optics theory describing the quantum interaction of light with subrelativistic free electrons,[138] opening up a path to free-electron quantum optics. Q-PINEM theory gener-

alizes the electron–photon interaction into the strong coupling regime and predicts the coupling between free electrons and an empty cavity, which has been confirmed in experiments.[139] Adopting Q-PINEM theory and designed high-efficiency silicon photonic nanostructures, Kaminer and co-workers found that quantum photon statistics can be imprinted on the free-electron–photon interaction, demonstrating the ability to reconstruct photon statistics from electron energy spectra.[140,141] In addition, by exploiting the entanglement between electrons and photons, it is possible to shape quantum photonic states[142] and to induce entanglement between photons[143] using free electrons. Further theoretical investigations have been carried out in PINEM, including those on the reconstruction of the quantum wave function of an electron pulse,[144] the use of PINEM electrons to perform quantum simulations[145] and ghost imaging,[146] and the free-electron qubit.[147,148]

7. Summary and outlook

We summarized the applications of the versatile UTEM with diffraction, imaging, and spectroscopy in the dynamic probing of a lattice, electron, and spin system of a material upon ultrafast laser excitation. In particular, ultrafast real-space imaging with nanometer–picosecond resolution makes it possible to experimentally visualize ultrafast processes with spatial inhomogeneity in the sample and to determine the local effect on the structural dynamics. Until now, ultrafast ångström-scale atomic imaging has not been realized, mainly owing to the contradiction between the single-pulse electron dose (i.e., the signal-to-noise ratio) and spatial–temporal resolution limited by the space-charge effect, and also the adverse effects of photothermal accumulation and photomechanical instability for excitation at a high repletion rate. The ultrafast spatial resolution can be improved using a pulsed electron source with higher spatiotemporal coherence, new imaging method (e.g., electron ptychography[1]), and a camera having extremely low noise (e.g., a pixel-array detector) that allows a long exposure time for accumulating a sufficiently strong signal. Several approaches, namely the adoption of radio-frequency or terahertz pulse compression, relativistic MeV electron imaging, an energy-filtered UTEM, and a laser-free stroboscopic UTEM based on beam blanking, offer further opportunities to extend the performance and expand the application space of the UTEM.

Exciting electrons in quantum materials with light pulses provide the possibility of generating new states that do not result from laser-induced heating effects but rather emerge from inherently nonthermal microscopic processes, such as new CDW hidden state and magnetic texture. Combined with the *in-situ* technique of the TEM (involving cooling, an electric/magnetic field, and strain) and ultrafast laser excitation with varying pulse energy, wavelength, polarization, and even phase, the UTEM is used to nonthermally control the macroscopic properties of quantum materials and characterize the structure of a new state.

As a promising new method, using the interaction between free electrons and optical near fields, PINEM is extensively used for real-space near-field imaging and free-electron wave packet shaping. Both theoretical and experimental advances in PINEM were summarized in the present review. Besides the subrelativistic electrons of the UTEM, the interaction of slow electrons with near fields has been studied both theoretically and experimentally.[149,150] In summary, PINEM has evolved both as an imaging technique and as a tool for electron phase modulation, and the development of free-electron quantum optics provides another method for controlling the electron wave function. With the advance of experimental technology and the proposal of new schemes, the UTEM will be developed into an efficient tool for exploring quantum mechanisms and ultrafast processes.

Acknowledgements

This project was supported by the National Natural Science Foundation of China (Grant Nos. U22A6005 and 12074408), the National Key Research and Development Program of China (Grant No. 2021YFA1301502), Guangdong Major Scientific Research Project (Grant No. 2018KZDXM061), Youth Innovation Promotion Association of CAS (Grant No. 2021009), Scientific Instrument Developing Project of the Chinese Academy of Sciences (Grant Nos. YJKYYQ20200055, ZDKYYQ2017000, and 22017BA10), Strategic Priority Research Program (B) of the Chinese Academy of Sciences (Grant Nos. XDB25000000 and XDB33010100), Beijing Municipal Science and Technology Major Project (Grant No. Z201100001820006), IOP Hundred Talents Program (Grant No. Y9K5051), Postdoctoral Support Program of China (Grant No. 2020M670501), and the Synergetic Extreme Condition User Facility (SECUF).

References

[1] Chen Z, Jiang Y, Shao Y T, Holtz M E, Odstrčil M, Guizar-Sicairos M, Hanke I, Ganschow S, Schlom D G and Muller D A 2021 *Science* **372** 826
[2] Krivanek O L, Dellby N, Hachtel J A, Idrobo J C, Hotz M T, Plotkin-Swing B, Bacon N J, Bleloch A L, Corbin G J, Hoffman M V, Meyer C E and Lovejoy T C 2019 *Ultramicroscopy* **203** 60
[3] Vanacore G M, Fitzpatrick A W P and Zewail A H 2016 *Nano Today* **11** 228
[4] Arbouet A,Caruso G M and Houdellier F 2018 *Ultrafast Transmission Electron Microscopy: Historical Development, Instrumentation and Applications* (London: Elsevier) pp. 1–72
[5] Caruso G M, Houdellier F, Weber S, Kociak M and Arbouet A 2019 *Adv. Phys. X* **4** 1660214
[6] Park S T, Flannigan D J and Zewail A H 2012 *J. Am. Chem. Soc.* **134** 9146
[7] Vanacore G M, van der Veen R M and Zewail A H 2015 *ACS Nano* **9** 1721

[8] Li Z, Xiao R J, Xu P, Zhu C, Sun S, Zheng D, Wang H, Zhang M, Tian H, Yang H X and Li J Q 2019 *ACS Nano* **13** 11623
[9] Horstmann J G,Böckmann H, Wit B, Kurtz F, Storeck G and Ropers C 2020 *Nature* **583** 232
[10] Valley D T, Ferry V E and Flannigan D J 2016 *Nano Lett.* **16** 7302
[11] Zhang Y and Flannigan D J 2021 *Nano Lett.* **21** 7332
[12] Gnabasik R A, Suri P K, Chen J and Flannigan D J 2022 *Phys. Rev. M* **6** 024802
[13] Tong L, Yuan J, Zhang Z, Tang J and Wang Z 2023 *Nat. Nanotechnol.* **18** 145
[14] Su Z, Baskin J S, Zhou W, Thomas J M and Zewail A H 2017 *J. Am. Chem. Soc.* **139** 4916
[15] Park S T, Lin M M and Zewail A H 2010 *New. J. Phys.* **12** 123028
[16] Feist A, Echternkamp K E, Schauss J, Yalunin S V, Schäfer S and Ropers C 2015 *Nature* **521** 200
[17] Zewail A H 2010 *Science* **328** 187
[18] Zhu C, Zheng D, Wang H, Zhang M, Li Z, Sun S, Xu P, Tian H, Li Z, Yang H and Li J 2020 *Ultramicroscopy* **209** 112887
[19] Barwick B, Park H S, Kwon O H, Baskin J S and Zewail A H 2008 *Science* **322** 1227
[20] Piazza L, Masiel D J, LaGrange T, Reed B W, Barwick B and Carbone F 2013 *Chem. Phys.* **423** 79
[21] Cao G, Sun S, Li Z, Tian H, Yang H and Li J 2015 *Sci. Rep.* **5** 8404
[22] Bücker K, Picher M, Crégut O, LaGrange T, Reed B W, Park S T, Masiel D J and Banhart F 2016 *Ultramicroscopy* **171** 8
[23] Ji S, Piazza L, Cao G, Park S T, Reed B W, Masiel D J and Weissenrieder J 2017 *Struct. Dyn.* **4** 054303
[24] Feist A, Bach N, Rubiano da Silva N, Danz T, Möller M, Priebe K E, Domröse T, Gatzmann J G, Rost S, Schauss J, Strauch S, Bormann R, Sivis M, Schäfer S and Ropers C 2017 *Ultramicroscopy* **176** 63
[25] Caruso G M, Houdellier F, Abeilhou P and Arbouet A 2017 *Appl. Phys. Lett.* **111** 023101
[26] Olshin P K, Drabbels M and Lorenz U J 2020 *Struct. Dyn.* **7** 054304
[27] Feist A, Rubiano da Silva N, Liang W, Ropers C and Schäfer S 2018 *Struct. Dyn.* **5** 014302
[28] Houdellier F, Caruso G M, Weber S, Kociak M and Arbouet A 2018 *Ultramicroscopy* **186** 128
[29] Verhoeven W, van Rens J F M, Kemper A H, Rietman E H, van Doorn H A, Koole I, Kieft E R, Mutsaers P H A and Luiten O J 2019 *Rev. Sci. Instrum.* **90** 083703
[30] Fu X, Wang E, Zhao Y, Liu A, Montgomery E, Gokhale V J, Gorman J J, Jing C, Lau J W and Zhu Y 2020 *Sci. Adv.* **6** eabc3456
[31] Yang J, Yoshida Y and Yasuda H 2018 *Microscopy* **67** 291
[32] Lu C, Jiang T, Liu S, Wang R, Zhao L, Zhu P, Liu Y, Xu J, Yu D, Wan W, Zhu Y, Xiang D and Zhang J 2018 *Appl. Phys. Lett.* **112** 113102
[33] van Oudheusden T, Pasmans P L E M, van der Geer S B, de Loos M J, van der Wiel M J and Luiten O J 2010 *Phys. Rev. Lett.* **105** 264801
[34] Gliserin A, Walbran M, Krausz F and Baum P 2015 *Nat. Commun.* **6** 8723
[35] Sun S, Sun X, Bartles D, Wozniak E, Williams J, Zhang P and Ruan C Y 2020 *Struct. Dyn.* **7** 064301
[36] Kealhofer C, Schneider W, Ehberger D, Ryabov A, Krausz F and Baum P 2016 *Science* **352** 429
[37] Ehberger D, Mohler K J, Vasileiadis T, Ernstorfer R, Waldecker L and Baum P 2019 *Phys. Rev. Appl.* **11** 024034
[38] Zhang Y, Li Z, Li Z, Li J, Li J and Yang H 2022 *J. Phys. Chem. C* **126** 20929
[39] La Grange T, Reed B W and Masiel D J 2015 *MRS Bull.* **40** 22
[40] Montgomery E, Leonhardt D and Roehling J 2021 *Micros. Today* **29** 46
[41] Filippetto D, Musumeci P, Li R K, Siwick B J, Otto M R, Centurion M and Nunes J P F 2022 *Rev. Mod. Phys.* **94** 045004
[42] Shimojima T,Nakamura A and Ishizaka K 2023 *Microscopy* **72** 287
[43] Zong A, Kogar A and Gedik N 2021 *MRS Bull.* **46** 720
[44] Sun X, Sun S and Ruan C Y 2021 *C. R. Phys.* **22** 15
[45] Li Z, Sun S, Li Z A, Zhang M, Cao G, Tian H, Yang H and Li J 2017 *Nanoscale* **9** 13313
[46] Sun S, Li Z, Li Z A, Xiao R, Zhang M, Tian H, Yang H and Li J 2018 *Nanoscale* **10** 7465
[47] Chatelain R P, Morrison V R, Klarenaar B L M and Siwick B J 2014 *Phys. Rev. Lett.* **113** 235502
[48] Mannebach E M, Nyby C, Ernst F, *et al.* 2017 *Nano Lett.* **17** 7761
[49] Chebl M, He X and Yang D S 2022 *Nano Lett.* **22** 5230
[50] Karam T E, Hu J and Blake G A 2018 *ACS Photonics* **5** 1228
[51] Wei L, Sun S, Guo C, Li Z, Sun K, Liu Y, Lu W, Sun Y, Tian H, Yang H and Li J 2017 *Struct. Dyn.* **4** 044012
[52] Zhang Y and Flannigan D J 2019 *Nano Lett.* **19** 8216
[53] Flannigan D J, Curtis W A, VandenBussche E J and Zhang Y 2022 *J. Chem. Phys.* **157** 180903
[54] Kim Y J, Lee Y, Kim K and Kwon O H 2020 *ACS Nano* **14** 11383
[55] Nakamura A, Shimojima T, Chiashi Y, Kamitani M, Sakai H, Ishiwata S, Li H and Ishizaka K 2020 *Nano Lett.* **20** 4932
[56] Eichberger M, Schäfer H, Krumova M, Beyer M, Demsar J, Berger H, Moriena G, Sciaini G and Miller R J D 2010 *Nature* **468** 799
[57] Han T R T, Zhou F, Malliakas C D, Duxbury P M, Mahanti S D, Kanatzidis M G and Ruan C Y 2015 *Sci. Adv.* **1** e1400173
[58] Vogelgesang S, Storeck G, Horstmann J G, Diekmann T, Sivis M, Schramm S, Rossnagel K, Schäfer S and Ropers C 2018 *Nat. Phys.* **14** 184
[59] Zong A, Shen X, Kogar A, Ye L, Marks C, Chowdhury D, Rohwer T, Freelon B, Weathersby S, Li R, Yang J, Checkelsky J, Wang X and Gedik N 2018 *Sci. Adv.* **4** eaau5501
[60] Zhou F, Williams J, Sun S, Malliakas C D, Kanatzidis M G, Kemper A F and Ruan C Y 2021 *Nat. Commun.* **12** 566
[61] Liu Q M, Wu D, Li Z A, Shi L Y, Wang Z X, Zhang S J, Lin T, Hu T C, Tian H F, Li J Q, Dong T and Wang N L 2021 *Nat. Commun.* **12** 2050
[62] Sun S, Wei L, Li Z, Cao G, Liu Y, Lu W J, Sun Y P, Tian H, Yang H and Li J 2015 *Phys. Rev. B* **92** 224303
[63] Sun K, Sun S, Zhu C, Tian H, Yang H and Li J 2018 *Sci. Adv.* **4** eaas9660
[64] Danz T,Domröse T and Ropers C 2021 *Science* **371** 371
[65] Stojchevska L, Vaskivskyi I, Mertelj T, Kusar P, Svetin D, Brazovskii S and Mihailovic D 2014 *Science* **344** 177
[66] Zhang M, Cao G, Tian H, Sun S, Li Z, Li X, Guo C, Li Z, Yang H and Li J 2017 *Phys. Rev. B* **96** 174203
[67] Zhang M, Li Z A, Sun S, Xu P, Zhu C, Tian H, Li Z, Zhang Y, Yang H and Li J 2019 *Phys. Rev. Appl.* **12** 034037
[68] Baum P, Yang D S and Zewail A H 2007 *Science* **318** 788
[69] Morrison V R, Chatelain R P, Tiwari K L, Hendaoui A, Bruhács A, Chaker M and Siwick B J 2014 *Science* **346** 445
[70] Sood A, Shen X, Shi Y, Kumar S, Park S J, Zajac M, Sun Y, Chen L Q, Ramanathan S, Wang X, Chueh W C and Lindenberg A M 2021 *Science* **373** 352
[71] Zhang M, Li Z A, Tian H, Yang H and Li J 2018 *Appl. Phys. Lett.* **113** 133103
[72] Kim Y J, Nho H W, Ji S, Lee H, Ko H, Weissenrieder J and Kwon O H 2023 *Sci. Adv.* **9** eadd5375
[73] Harvey T, Silva N, Gaida J, Möller M, Feist A, Schäfer S and Ropers C 2021 *MRS Bull.* **46** 711
[74] Shimojima T, Nakamura A, Yu X, Karube K, Taguchi Y, Tokura Y and Ishizaka K 2021 *Sci. Adv.* **7** eabg1322
[75] Tengdin P, Truc B, Sapozhnik A, Kong L, del Ser N, Gargiulo S, Madan I, Schönenberger T, Baral P R, Che P, Magrez A, Grundler D, Rønnow H M, Lagrange T, Zang J, Rosch A and Carbone F 2022 *Phys. Rev. X* **12** 041030
[76] Giannetti C, Capone M, Fausti D, Fabrizio M, Parmigiani F and Mihailovic D 2016 *Adv. Phys.* **65** 58
[77] Orenstein J 2012 *Phys. Today* **65** 44
[78] Carbone F, Hengsberger M, Castiglioni L and Osterwalder J 2017 *Struct. Dyn.* **4** 061504
[79] Egerton R F 2011 *Electron Energy-Loss Spectroscopy in Electron Microscopy* (3rd edn.) (New York: Springer) pp. 1–26
[80] Liu H, Baskin J S and Zewail A H 2016 *Proc. Natl. Acad. Sci. USA* **113** 2041
[81] Carbone F, Kwon O H and Zewail A H 2009 *Science* **325** 181
[82] Carbone F 2010 *Chem. Phys. Lett.* **496** 291
[83] Piazza L, Ma C, Yang H X, Mann A, Zhu Y, Li J Q and Carbone F 2013 *Struct. Dyn.* **1** 014501
[84] Zheng D, Zhu C, Li Z, Li Z, Li J, Sun S, Zhang Y, Wang F, Tian H, Yang H and Li J 2020 *Nanoscale Adv.* **2** 2808
[85] van der Veen R M, Penfold T J and Zewail A H 2015 *Struct. Dyn.* **2** 024302
[86] Carbone F 2015 *Struct. Dyn.* **2** 020601
[87] Pomarico E, Kim Y J, de Abajo F J G, Kwon O H, Carbone F and van der Veen R M 2018 *MRS Bull.* **43** 497

[88] Hassan M T, Liu H, Baskin J S and Zewail A H 2015 *Proc. Natl. Acad. Sci. USA* **112** 12944
[89] Fu X, Barantani F, Gargiulo S, Madan I, Berruto G, LaGrange T, Jin L, Wu J, Vanacore G M, Carbone F and Zhu Y 2021 *Nat. Commun.* **12** 2123
[90] Zheng D, Huang S, Zhu C, Li Z, Zhang Y, Yang D, Tian H, Li J, Yang H and Li J 2022 *Nanoscale* **14** 10477
[91] Barwick B, Flannigan D J and Zewail A H 2009 *Nature* **462** 902
[92] Javier Garcia de Abajo F, Asenjo-Garcia A and Kociak M 2010 *Nano Lett.* **10** 1859
[93] Pomarico E, Madan I, Berruto G, Vanacore G M, Wang K, Kaminer I, Garcia de Abajo F J and Carbone F 2018 *ACS Photonics* **5** 759
[94] Hassan M T, Baskin J S, Liao B and Zewail A H 2017 *Nat. Photonics* **11** 425
[95] Yurtsever A, van der Veen R M and Zewail A H 2012 *Science* **335** 59
[96] Yurtsever A, Baskin J S and Zewail A H 2012 *Nano Lett.* **12** 5027
[97] Yurtsever A and Zewail A H 2012 *Nano Lett.* **12** 3334
[98] Piazza L, Lummen T T A, Quinonez E, Murooka Y, Reed B W, Barwick B and Carbone F 2015 *Nat. Commun.* **6** 6407
[99] Fu X, Sun Z, Ji S, Liu F, Feng M, Yoo B K and Zhu Y 2022 *Nano Lett.* **22** 2009
[100] Flannigan D J, Barwick B and Zewail A H 2010 *Proc. Natl. Acad. Sci. USA* **107** 9933
[101] Huang S, Xu P, Zheng D, Li J, Tian H, Yang H and Li J 2023 *Appl. Phys. Lett.* **122** 111102
[102] Madan I, Vanacore G M, Pomarico E, Berruto G, Lamb R J, McGrouther D, Lummen T T A, Latychevskaia T, Garcia de Abajo F J and Carbone F 2019 *Sci. Adv.* **5** eaav8358
[103] Lummen T T A, Lamb R J, Berruto G, LaGrange T, Dal Negro L, Garcia de Abajo F J, McGrouther D, Barwick B and Carbone F 2016 *Nat. Commun.* **7** 13156
[104] Konecna A, Di Giulio V, Mkhitaryan V, Ropers C and Garcia de Abajo F J 2020 *ACS Photonics* **7** 1290
[105] Zheng D, Huang S, Zhu C, Xu P, Li Z, Wang H, Li J, Tian H, Yang H and Li J 2021 *Nano Lett.* **21** 10238
[106] Wang K, Dahan R, Shentcis M, Kauffmann Y, Ben Hayun A, Reinhardt O, Tsesses S and Kaminer I 2020 *Nature* **582** 50
[107] Kfir O, Lourenco-Martins H, Storeck G, Sivis M, Harvey T R, Kippenberg T J, Feist A and Ropers C 2020 *Nature* **582** 46
[108] Yannai M, Dahan R, Gorlach A, Adiv Y, Wang K, Madan I, Gargiulo S, Barantani F, Dias E J C, Vanacore G M, Rivera N, Carbone F, de Abajo F J G and Kaminer I 2023 *ACS Nano* **17** 3645
[109] Madan I, Dias E J C, Gargiulo S, Barantani F, Yannai M, Berruto G, LaGrange T, Piazza L, Lummen T T A, Dahan R, Kaminer I, Vanacore G M, de Abajo F J G and Carbone F 2023 *ACS Nano* **17** 3657
[110] Kurman Y, Dahan R, Sheinfux H H, Wang K, Yannai M, Adiv Y, Reinhardt O, Tizei L H G, Woo S Y, Li J, Edgar J H, Kociak M, Koppens F H L and Kaminer I 2021 *Science* **372** 1181
[111] Echternkamp K E, Feist A, Schafer S and Ropers C 2016 *Nat. Phys.* **12** 1000
[112] Henke J W, Raja A S, Feist A, Huang G, Arend G, Yang Y, Kappert F J, Wang R N, Moller M, Pan J, Liu J, Kfir O, Ropers C and Kippenberg T J 2021 *Nature* **600** 653
[113] Adiv Y, Wang K, Dahan R, Broaddus P, Miao Y, Black D, Leedle K, Byer R L, Solgaard O, England R J and Kaminer I 2021 *Phys. Rev. X* **11** 041042
[114] Shiloh R, Schoenenberger N, Adiv Y, Ruimy R, Karnieli A, Hughes T, England R J, Leedle K J, Black D S, Zhao Z, Musumeci P, Byer R l, Arie A, Kaminer I and Hommelhoff P 2022 *Adv. Opt. Photonics* **14** 862
[115] Tsesses S, Dahan R, Wang K, Bucher T, Cohen K, Reinhardt O, Bartal G and Kaminer I 2023 *Nat. Mater.* **22** 345
[116] Konecna A and Garcia de Abajo F J 2020 *Phys. Rev. Lett.* **125** 030801
[117] Polman A, Kociak M and García de Abajo F J 2019 *Nat. Mater.* **18** 1158
[118] Gliserin A, Apolonski A, Krausz F and Baum P 2012 *New. J. Phys.* **14** 073055
[119] Gover A and Pan Y 2018 *Phys. Lett. A* **382** 1550
[120] Pan Y, Zhang B and Gover A 2019 *Phys. Rev. Lett.* **122** 183204
[121] Priebe K E, Rathje C, Yalunin S V, Hohage T, Feist A, Schäfer S and Ropers C 2017 *Nat. Photonics* **11** 793
[122] Yang Y, Roques-Carmes C, Kooi S E, Tang H, Beroz J, Mazur E, Kaminer I, Joannopoulos J D and Soljacic M 2023 *Nature* **613** 42
[123] Morimoto Y and Baum P 2018 *Nat. Phys.* **14** 252
[124] Vanacore G M, Madan I, Berruto G, Wang K, Pomarico E, Lamb R J, McGrouther D, Kaminer I, Barwick B, Garcia de Abajo F J and Carbone F 2019 *Nat. Commun.* **10** 1069
[125] Morimoto Y and Baum P 2018 *Phys. Rev. A* **97** 033815
[126] Batelaan H 2007 *Rev. Mod. Phys.* **79** 929
[127] Freimund D L, Aflatooni K and Batelaan H 2001 *Nature* **413** 142
[128] Schwartz O, Axelrod J J, Campbell S L, Turnbaugh C, Glaeser R M and Mueller H 2019 *Nat. Methods* **16** 1016
[129] Feist A, Yalunin S V, Schäfer S and Ropers C 2020 *Phys. Rev. Res.* **2** 043227
[130] Vanacore G M, Berruto G, Madan I, Pomarico E, Biagioni P, Lamb R J, McGrouther D, Reinhardt O, Kaminer I, Barwick B, Larocque H, Grillo V, Karimi E, Garcia de Abajo F J and Carbone F 2019 *Nat. Mater.* **18** 573
[131] Uchida M and Tonomura A 2010 *Nature* **464** 737
[132] Verbeeck J, Tian H and Schattschneider P 2010 *Nature* **467** 301
[133] McMorran B J, Agrawal A, Anderson I M, Herzing A A, Lezec H J, McClelland J J and Unguris J 2011 *Science* **331** 192
[134] Garcia de Abajo F J, Barwick B and Carbone F 2016 *Phys. Rev. B* **94** 041404
[135] Cai W, Reinhardt O, Kaminer I and Garcia de Abajo F J 2018 *Phys. Rev. B* **98** 045424
[136] Madan I, Leccese V, Mazur A, Barantani F, LaGrange T, Sapozhnik A, Tengdin P M, Gargiulo S, Rotunno E, Olaya J C, Kaminer I, Grillo V, de Abajo F J G, Carbone F and Vanacore G M 2022 *ACS Photonics* **9** 3215
[137] Garcia de Abajo F J and Konecna A 2021 *Phys. Rev. Lett.* **126** 123901
[138] Kfir O 2019 *Phys. Rev. Lett.* **123** 103602
[139] Feist A, Huang G, Arend G, Yang Y, Henke J W, Raja A S, Kappert F J, Wang R N, Lourenco-Martins H, Qiu Z, Liu J, Kfir O, Kippenberg T J and Ropers C 2022 *Science* **377** 777
[140] Dahan R, Gorlach A, Haeusler U, Karnieli A, Eyal O, Yousefi P, Segev M, Arie A, Eisenstein G, Hommelhoff P and Kaminer I 2021 *Science* **373** eabj7128
[141] Di Giulio V, Kociak M and Garcia de Abajo F J 2019 *Optica* **6** 1524
[142] Ben Hayun A, Reinhardt O, Nemirovsky J, Karnieli A, Rivera N and Kaminer I 2021 *Sci. Adv.* **7** eabe4270
[143] Baranes G, Ruimy R, Gorlach A and Kaminer I 2022 *npj Quantum Inf.* **8** 32
[144] Chen Z, Zhang B, Pan Y and Krueger M 2023 *Sci. Adv.* **9** eadg8516
[145] Pan Y, Zhang B and Podolsky D 2022 arXiv:2207.07010 [quant-ph]
[146] Rotunno E, Gargiulo S, Vanacore G M, Mechel C, Tavabi A, Dunin Borkowski R E, Carbone F, Maidan I, Zanfrognini M, Frabboni S, Guner T, Karimi E, Kaminer I and Grillo V 2021 arXiv:2106.08955 [quant-ph]
[147] Reinhardt O, Mechel C, Lynch M and Kaminer I 2021 *Ann Phys.* **533** 2000254)
[148] Tsarev M V, Ryabov A and Baum P 2021 *Phys. Rev. Res.* **3** 043033
[149] Talebi N 2020 *Phys. Rev. Lett.* **125** 080401
[150] Shiloh R, Chlouba T and Hommelhoff P 2022 *Phys. Rev. Lett.* **128** 235301